Quasielastic electron scattering and Coulomb sum rule in ^{4}He

K. F. von Reden,* C. Alcorn, S. A. Dytman, and B. Lowry
Department of Physics, University of Pittsburgh, Pittsburgh, Pennsylvania 15260

B. P. Quinn
Department of Physics, Carnegie-Mellon University, Pittsburgh, Pennsylvania 15213

D. H. Beck,† A. M. Bernstein, K. I. Blomqvist,‡ G. Dodson, K. A. Dow, J. Flanz,
G. Retzlaff,§ C. P. Sargent, and W. Turchinetz
*Physics Department and Bates Linear Accelerator Center, Massachusetts Institute of Technology,
Cambridge, Massachusetts 02139*

M. Farkhondeh,** J. S. McCarthy, T. S. Ueng, and R. R. Whitney††
Department of Physics, University of Virginia, Charlottesville, Virginia 22901
(Received 27 June 1989)

Double differential cross sections for inelastic electron scattering from ^{4}He have been measured at bombarding energies between 279 and 725 MeV. The longitudinal and transverse response functions were obtained for constant momentum transfer between 300 and 500 MeV/c. Plane-wave impulse approximation calculations overestimate the longitudinal response and produce fair agreement with the transverse part. The Coulomb sum is determined and compared with exact calculations. Within the experimental error the data exhaust the sum rule; this provides a first measurement of ground-state correlations.

I. INTRODUCTION

Quasielastic scattering is one of the dominant reaction mechanisms in inelastic electron scattering at intermediate energies. A broad peak is observed in the (e,e') doubly differential cross section spectrum at an excitation energy of roughly $Q^2/2m$, where Q is the four-momentum transfer and m is the nucleon mass. The location of the peak suggests that electrons are elastically scattered from moving nucleons and the shape of the peak can then be interpreted as a reflection of the nucleon momentum distribution within the nucleus. A successful description[1] of quasielastic electron scattering cross sections for carbon and heavier nuclei used a nucleon momentum distribution derived from a zero-temperature Fermi gas model of the nucleus. However, more complete measurements[2] obtained a separation of the nuclear response into longitudinal and transverse parts, corresponding to scattering from charges and from spins and currents, respectively. When this was done, significant discrepancies between plane-wave impulse approximation (PWIA) calculations and the more detailed data[2] were found. These discrepancies have been attributed to effects not accounted for in the PWIA calculations such as multinucleon knock out, final-state interactions (FSI's), meson exchange currents (MEC's), and possible modification of the nucleon form factors in the nuclear medium (see Refs. 2, 3, and 5). Even though some of these effects may be large, a consistent improvement in the theoretical predictions of quasielastic electron scattering has not been achieved.

The problems encountered for heavier nuclei are probably largely due to the difficulty in accurately calculating initial- and final-state wave functions for many-body systems. During the past five years, a series of electron scattering experiments have been performed on $A = 2$-4 nuclei at the Bates Linear Accelerator Center with a goal of observing mechanisms deviating from the simple quasielastic scattering picture in nuclei for which calculations will be more reliable. Very sophisticated calculations are now available for the nuclear ground-state wave functions of $A = 2$-4 nuclei.

As the density of these nuclei rapidly increases from $A = 2$ to 4, the reaction mechanism should become more complicated due to final-state interactions and multinucleon ejections. For ^{2}H, the quasielastic peak[3] is symmetric and is described quite well by calculations[4] at all momentum transfers of interest here, 250–600 MeV/c. These calculations[4] include FSI's, MEC's, and pion production, but their influence on the results is less than 10% in the quasielastic peak region. Significant simplification results from the comparatively small binding energy and ability to generate FSI's with the same potential as the initial bound state. The three-body ground-state wave functions are reasonably well understood, but not the final states in the continuum that are populated in (e,e') experiments.[5] Although the Coulomb sum-rule (the total inelastic strength at a given momentum transfer) calculation[6-8] accurately fits the data, no present calculation can describe both the ^{3}H and ^{3}He data for the quasielastic peak. The worst agreement is for the longitudinal response function (where the discrepancies are roughly 30%) even though most higher-order effects should not be important.

^{4}He lies between the very light nuclei and the others in a number of ways. Although its wave function is becoming accessible via calculations[9,10] using realistic two- and

three-body interactions, it has a central matter density more typical of heavier nuclei. Higher-order effects should then be more important than in lighter nuclei. In addition, ^{4}He has excited states at 20–30 MeV that should influence the (e,e') spectrum. Thus, the (e,e') data for ^{4}He can provide a link to better understanding of the inelastic response in heavier nuclei.

A previous quasielastic electron scattering experiment on ^{2}H and ^{3,4}He was performed at the Bates Linear Accelerator[3] by many of the present authors. Based on that experience, a more extensive and accurate set of data was obtained for ^{2,3}H and ^{3,4}He.[5] This paper presents the new results for ^{4}He (e,e'). The following sections will discuss notation, experimental procedure, data analysis, and radiative corrections. The ^{4}He electron scattering cross sections and response functions obtained in this experiment are compared to PWIA calculations[11] based on realistic wave functions in Sec. VI.

The consideration of sum rules is an independent way to calculate the nuclear response to electromagnetic interactions directly from ground-state expectation values assuming closure.[9,12] Such calculations avoid the problem of the treatment of final-state interactions and are exact on the basis of realistic ground-state wave functions. Of particular interest is the question of whether or not pair correlations exist in the nuclear ground state. In the case of ^{3}H and ^{3}He such correlations have clearly been observed.[5] In Sec. VII, ^{4}He results will be presented in comparison with calculations by the Illinois group.[9]

II. KINEMATICS

Under the assumption of parity conservation, Lorentz invariance, and gauge invariance, double-differential cross sections for inclusive electron scattering can be written[12] in terms of kinematic factors and angle-independent longitudinal and transverse response functions, R_L and R_T, that contain all the nuclear structure information:

$$\frac{d^2\sigma}{d\Omega\,dE_f} = \sigma_{\text{Mott}}[v_L R_L(q,\omega) + v_T R_T(q,\omega)] \ ,$$

$$v_L = \left[\frac{Q^2}{q^2}\right]^2 \ ,$$

$$v_T = \left[\frac{1}{2}\left|\frac{Q^2}{q^2}\right| + \tan^2\frac{\theta}{2}\right] \ ,$$

$$\sigma_{\text{Mott}} = \frac{\alpha^2\cos^2(\theta/2)}{4E_i^2\sin^4(\theta/2)} \ ,$$

where q and $\omega = E_i - E_f$ are the three momentum and energy lost by the electron in the scattering, Q is the four-momentum transfer with

$$Q^2 = \omega^2 - q^2 = -4E_i E_f\sin^2(\theta/2) \ ,$$

θ is the lab electron scattering angle, and E_i and E_f are the incident and scattered electron energy, respectively. By measuring the cross sections for at least two angles, preferably including both forward and backward angles, the two response functions R_L and R_T can be separated,

as will be discussed later. Figure 1 shows the region of the (q,ω) plane covered by this experiment. Dashed and solid curves represent the lines of constant incident energy (labeled for each curve) for the forward (60°) and backward (134.5°) angle measurements, respectively. Also shown are curves depicting the position of the elastic scattering peak for ^{4}He and ^{1}H and the photon line $(q=\omega)$, dividing the spacelike and timelike regions.

III. EXPERIMENT

The electron scattering experiment was conducted at the Bates Linear Accelerator using the 900 MeV energy-loss spectrometer system (ELSSY).[13] The electron beam of up to 20 μA average current (duty factor 1%) was passed through a gas cell filled with ^{4}He, pressurized to 1552 kPa (225 psi) (absolute) at 45 K. During this run cycle, a second identical cell was filled with either ^{2}H or ^{1}H. Results for ^{2}H are reported elsewhere.[14] Electrons scattered from the target were measured at two spectrometer angle settings and seven incident energy values: 60°; 365, 476, 589, and 725 MeV and 134.5°; 279, 328, and 368 MeV. In order to cover excitation energies up to the onset of the Δ(1232) resonance, a series of measurements had to be taken at each angle/energy combination because of the limited (6%) momentum acceptance of ELSSY. For a number of settings, elastic scattering was also measured for calibration and normalization purposes.
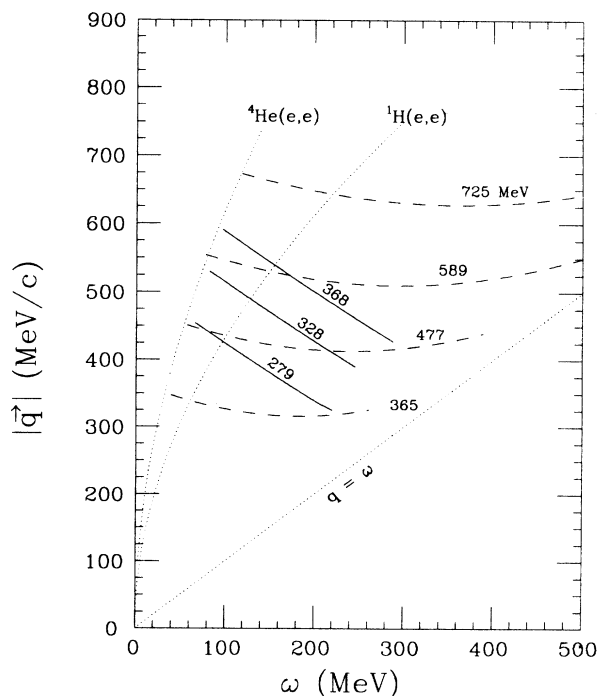

FIG. 1. Electron scattering kinematics. The lines of constant incident energy are labeled with the energy value. Dashed curves represent the 60° measurements, solid curves the 134.5° ones. Lines depicting the positions of the elastic scattering peaks of ^{4}He and ^{1}H, and the photon line $(q=\omega)$ are also shown.

The target system[15] was developed for measurements of electron scattering from light nuclei, including ^{3}H gas. Although the elaborate safety precautions required for ^{3}H were not necessary in this experiment, the same containment system was used as a test. A detailed description of the system can be found elsewhere.[15] Each of the three target cells (two filled with gas, one evacuated for background measurements) was a 4.45 cm high cylindrical container of 10.2 cm diameter (axis vertical, perpendicular to the beam axis), made of .127 μm thick Elgiloy[16] (an alloy of mainly Ni, Cr, and Co) with stainless-steel endplates. Surrounding each cell were two aluminum containers with 0.25 mm windows. A 0.035 g/cm^2 BeO screen was mounted in the entrance passage of the system. The total window thickness was 2% of a radiation length on the entrance side and 1.4% of a radiation length on the exit side. At a gas density of about 0.107 g/cm^3, the contribution to the radiation length on entrance and exit was $\leq 0.1\%$ for the ^{4}He gas. The target cell was equipped with a heater, ^{4}He gas refrigeration, and redundant pressure and temperature transducers. The gas density was continuously monitored during the experiment by recording pressure and temperature in short time intervals. Given the pressure, temperature, and accurate knowledge of the volumes involved in the filling procedure, the virial equation of state was employed to calculate the target density using coefficients from Ref. 17. Each time the cell was filled and during extended interrupts of the experiment, measurements of the gas density were performed by heating the target up to the vicinity of the operating point without beam on the target for periods of about 1 h. Beam heating effects were found to be negligible (less than 1% effect). This is less than was seen in previous experience at Bates because the beam was tuned to a more diffuse spot than normal. The target system was operated and controlled completely via a VAX computer/microcomputer system, independent of the data taking system.

Two sets of horizontal slits and one vertical slit determined the aperture of the spectrometer and the effective target length. The ELSSY focal plane instrumentation consisted of a vertical drift chamber (VDC), a pair of multiwire proportional counters [transverse array (TA)], and as trigger counters a 0.635 cm NE110 plastic scintillator and a Freon 12 gas Čerenkov counter [$n = 1.003$ at 276 kPa (40 psi) (absolute), resulting in a Čerenkov radiation threshold for pions of about 1.8 GeV/c]. The VDC measured the position of the dispersed electrons (i.e., their momentum) as well as the angle of the tracks in the focal plane with respect to the central ray. The multiwire proportional chambers (MWPC's) measured the position in the focal plane perpendicular to the dispersion direction, which is proportional to the scattering angle in the optics of the ELSSY.

A 2-of-3 majority logic coincidence signal was used for an event trigger, composed of the responses of the TA, scintillator, and Čerenkov detectors. The 2-of-3 majority logic allowed monitoring the trigger efficiency. In the final analysis, each of the three detectors had an efficiency of at least 98%. The coincidence signal was used as a time fiducial for the wire chamber delay line readout,

with the timing determined by the Čerenkov signal or in its absence by the scintillator signal.

IV. DATA ANALYSIS

Event records containing time information from the wire chambers, pulse heights from the scintillator and Čerenkov counters, and target monitoring information were digitized in computer-aided measurement and control (CAMAC) modules and passed via a microprogrammable branch driver (MBD II) to a Digital Equipment Corp. PDP 11-45 computer, running a data acquisition code under the RT-11 operating system. The raw data were buffered and written to magnetic tape for later replay. The data were also analyzed on line and histogrammed for monitoring purposes.

The raw data were corrected for background contributions. The main source of the background was identified to be the scattering of electrons from the target container. This was very small (about 1%) at the quasielastic peak because the target defining slits masked the target walls. At each field setting, data were taken on the empty target and the normalized counts were subtracted bin by bin from the gas target data. A second source of background was determined by inspection of the transverse array spectra. After subtraction of the empty target TA data from the gas target TA data, counts were still found in regions outside the geometrically allowed limits of the horizontal opening angle distribution that is measured in the TA. With two slits, this spectrum must have a trapezoidal shape for particles produced in the target volume. Since this background process was seen solely at large inelasticity and its cross section was very similar for both electrons and positrons, the source is very likely pair production. Based on the results of a large number of test runs, we believe the major source is showering of scattered electrons in the first set of horizontal slits. These data indicated a more or less flat shape for this background in the TA spectrum. Therefore, a flat distribution was assumed here and fitted to the TA spectra. An amount proportional to that background was subtracted from the gas target run data. This type of background was less than 1% under the quasielastic peak in general and grew to 10–20% at the highest scattered electron energy values.

In the replay, a number of efficiency corrections were made to account for certain conditions of the data acquisition system that led to an unwanted reduction of the number of "good" events recorded. First, a computer deadtime prevented all data buffers from being written to tape at high data rates. However, their number was recorded and a correction factor (almost always less than 3%) was applied on the basis of the ratio of good to rejected events in the buffers processed. Second, a rare double pulsing of the Čerenkov detector led to the rejection of typically 1–2% of good events. Third, for each event an enforced wire chamber deadtime of 300 ns would lead to a reduction in the number of good events at high data rates. Since, in this experiment, data rates were kept to less than one real event per beam burst of 15 μs, this correction was negligible. With the 2 of 3 majority

logic, the trigger efficiency was very close to 100% since each of the detectors was at least 98% efficient. Fourth, events that were marginally inconsistent because of the lack of one of the detector signals, were included in the data stream after careful analysis. Their occurrence was never more than 5% of the good event totals.

The electron counts were converted into a double-differential cross section:

$$\frac{d^2\sigma}{d\Omega\,dE_f} = \frac{N'_e F_{\text{eff}}}{N_e^0 \Delta E \rho \Delta \phi \langle l(\theta) d\theta \rangle} \ ,$$

where N'_e is the background-subtracted number of electrons found in energy bite ΔE, F_{eff} is the total efficiency correction described before, and N_e^0, ρ, and $\Delta\phi$ are the number of incident electrons, the target density, and the vertical angular acceptance, respectively. $\langle l(\theta)d\theta \rangle$ is the mean horizontal acceptance of the spectrometer for scattered electrons, originating from locations in the extended gas target,

$$l(\theta_{\min}) \leq l(\theta) \leq l(\theta_{\max}) \ ,$$

as determined by the two sets of horizontal slits. This quantity was evaluated with a numerical expression.[3] The statistical error of the cross section varied between 2% and 4%. The absolute error of about 8% is dominated by the uncertainty of the target density.

V. RADIATIVE CORRECTIONS

In the analysis of electromagnetic scattering data, considerable effort has to go into corrections for radiative processes. Electrons are subject to energy loss by bremsstrahlung either in the entrance passage or the exit passage of the target system (external processes) or in the field of the target nuclei themselves (internal processes). This leads to the unwanted result that either the incident energy of the electrons may not be the accelerator set value or scattered electrons have a lower energy than determined by the final state of the target, or both of the effects combined. In a measured spectrum, some of the scattered electrons therefore appear at a lower final energy than scattering from the target nucleus would otherwise yield. Another complication is the change of the scattering angle due to the radiation by the electrons. To correct for these radiative processes, two important assumptions can be made. First, calculations show that photons are only emitted by the electrons in the extreme forward direction (angle peaking approximation[18]). The data were corrected here assuming that the scattering angle is unchanged. Second, although many soft photons are emitted by an electron, almost all of the energy lost to radiation is carried away by a single hard photon (energy peaking approximation[18]). This approximation allows a separation of radiation losses prior to scattering from losses after scattering and exclusion of double losses.

The radiation correction procedure was started with the subtraction of the radiation tail of the elastic scattering peak from the inelastic continuum. The quality of the radiation tail prediction[18] was checked with a ^{1}H target,

which has no inelastic contribution below the pion production threshold. Figure 2 shows the ^{1}H spectrum for $E = 365$ MeV, $\theta = 60°$, together with the tail calculation. The known sources for bremsstrahlung in the entrance and exit passage of the target assembly appear to reasonably reproduce the data.

At several energy-angle combinations, elastic scattering data were taken from ^{4}He with 5% statistical error. This was done to check the absolute cross section calibration of the spectrometer and gas target setups. Agreement was found with previously published results[19] within the experimental error of the respective measurements.

Next, the radiative corrections for a bin in final energy in the continuum were calculated. In addition to scattered electrons with the correct kinematics for this bin that have not undergone any radiative processes, the following types of background can be found: Electrons that were initially scattered to a higher final energy value but then lost energy after scattering because of bremsstrahlung and electrons that lost energy before the scattering and then scattered into the present bin. After subtracting these background counts, the remaining counts have to be corrected for electrons that were initially scattered into this bin but then lost energy after scattering to bremsstrahlung. Although the amounts to be subtracted and added are sometimes very similar, the general feature of the radiative correction is that inelastic strength is transferred from the dip to the quasielastic peak. There is one further complication: knowledge of the inelastic scattering cross sections over the entire relevant section of the response surface is, in principle, required to do the aforementioned corrections properly. That, however, is just what we want to measure. Therefore, the uncorrected spectra measured in this experiment are assumed to be a zeroth order approximation of the true response surface that was then obtained by iteration. Corrections were applied to the spectra by interpolating and, to a small degree, extrapolating the measured cross sections to the kinematic points needed for the corrections. For the lower beam energies, data from our previous experiment[3] were
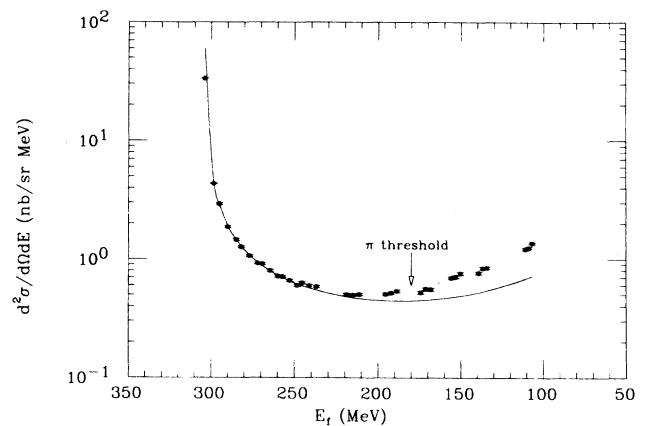
FIG. 2. ^{1}H elastic electron scattering spectrum at $E = 365$ MeV and $\theta = 60°$. The solid curve is the tail calculation using the formalism from Ref. 18.

used. By comparing inelastic cross sections measured at the same angle-energy combination, the absolute normalizations of the two experiments were shown to be less than 5% different. Then in the next step the first-order corrected data are substituted for the uncorrected cross sections, until after about 5–6 steps convergence to within 1% occurs.

In order to make the interpolations more accurate by removing the incident energy dependence of the measured cross sections, the data were reduced to the well-known scaling function

$$F(Y) = \frac{d^2\sigma}{d\Omega\, dE_f} \left[\sigma_{\text{Mott}} \frac{dY}{dE_f} (Z\sigma_{\text{ep}} + N\sigma_{\text{en}}) \right]^{-1},$$

using a simple nonrelativistic scaling variable

$$Y = \frac{M_N(E - E_f - E_B)}{q} - \frac{q}{2}.$$

Here $\sigma_{\text{ep,en}}$ are the eN cross sections, M_N is the nucleon mass, and E and E_f are the initial and final electron energies. E_B is an empirical constant that can be interpreted as an effective binding energy. In Fig. 3, we show the measured energy spectra plotted according to the preceding prescription. At the right side of the figure, the cross section is rising rapidly; the cross section no longer follows a common curve because the basic electron-nucleon interaction is pion production rather than elastic scattering. From other data,[5] it is also known that the measured scaling function decreases for both larger and smaller values of q than are sampled in the data shown here.

The corrected cross sections were finally separated into longitudinal and transverse response functions, R_L and R_T, at constant three-momentum transfers q between 300 and 500 MeV/c. In order to do this, cross sections at constant q were determined for the two angles using the interpolation procedures discussed earlier; the response functions were then obtained from a straight line fit to the quantity

$$\sigma_{\text{exp}} / [v_L \sigma_{\text{Mott}}(\theta)]$$
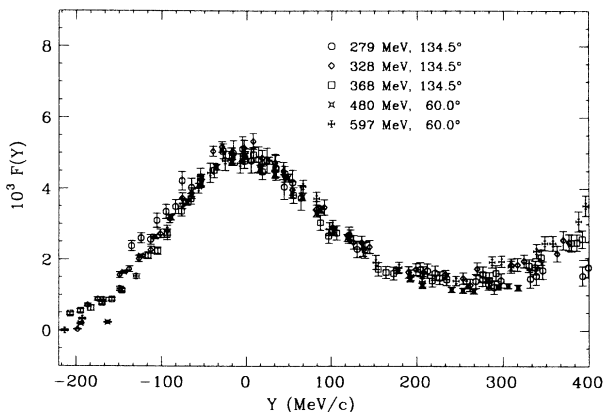
as a function of v_T / v_L.

FIG. 3. Y scaling for ^{4}He electron scattering cross sections measured in this experiment using a simple nonrelativistic scaling variable (see text).

VI. RESULTS

Examples of the radiatively corrected double-differential cross sections for inclusive electron scattering from ^{4}He at widely varying kinematic conditions are shown in Fig. 4. The error bars shown include the statistical contributions and a contribution from the radiative unfolding procedure. Calculations by the Rome group[11] are shown together with the data. The different curves represent the longitudinal and transverse components and the total cross sections. The calculation sums over all possible $(e,e'N)$ states using the plane-wave impulse approximation (PWIA) in the final state. The ^{4}He wave function used in Ref. 11 was calculated by Akaishi[10] employing the amalgamation of two-body correlations into multiple scattering (ATMS) method. It uses a three-body force to get the correct binding energy. For the electron-nucleon cross section, σ_{eN}, the off-shell formula $(cc1)$ by deForest[20] was used with form factors by Höhler *et al.*,[21] Blatnik and Zovko,[22] or Gari and Krüpelmann.[23] Only small differences ($\leq 3\%$) result from the choice of the form factors in the given range of momentum transfers. The agreement between data and calculations is best at high momentum transfer as might
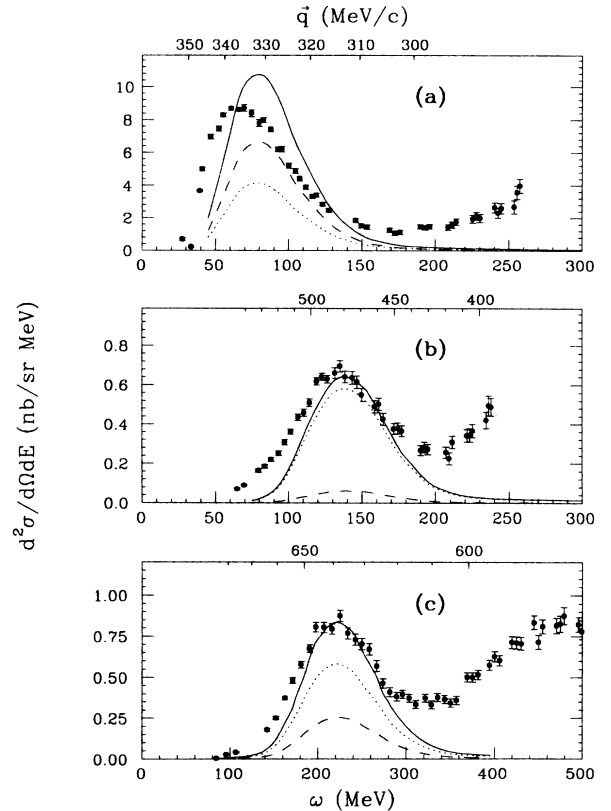

FIG. 4. Double-differential cross sections for electron scattering from ^{4}He at (a) $E = 365$ MeV, 60°; (b) $E = 328$ MeV, 134.5°; (c) $E = 725$ MeV, 60°; together with the PWIA calculations from Ref. 11. The dashed curves are the longitudinal contributions, the dotted curves are the transverse contributions, and the solid curves are the full cross sections. The three-momentum transfers are indicated on the top scales of the individual plots.

be expected for a PWIA model. At the lowest E, θ values Fig. 4(a) the calculations describe the reaction poorly. The asymmetric peak shape in the data suggests large contributions from excited states at 20–26 MeV. Final-state interactions (FSI's) were not taken into account but appear to be important in the ^{3}He and ^{3}H data.[5–8] Even at the higher-momentum transfers [Figs. 4(b) and (c)] the low excitation energy sides of the quasielastic peaks are still notably enhanced compared to the PWIA calculations. Effects of meson exchange currents (MEC's) and real pion production were also omitted in the calculations. Therefore the high excitation energy sides of the peaks are not expected to be reproduced by the calculations. Note the strong increase of the "dip" cross sections with momentum transfer, from $\approx 20\%$ of the peak value at 310 MeV/c to $\approx 30\%$ at 430 MeV/c to $\approx 50\%$ at 610 MeV/c.

Figure 5 demonstrates the relative contributions of the separated longitudinal and transverse components of the nuclear response to the measured cross sections at $E_{inc} = 589$ MeV, $\theta = 60°$. The momentum transfer at the quasielastic peak is about 530 MeV/c. Whereas the ratio of the transverse to the longitudinal response is about 2:1 at the peak, as expected from a PWIA calculation, the low and high ω tails of the peak are clearly dominated by the transverse component.

Separations of the measured cross sections into longitudinal and transverse response functions at constant momentum transfer are displayed in Fig. 6 together with the PWIA calculations by the Rome group[11] under the same conditions as discussed earlier. Here, the error bars reflect an additional contribution from the separation
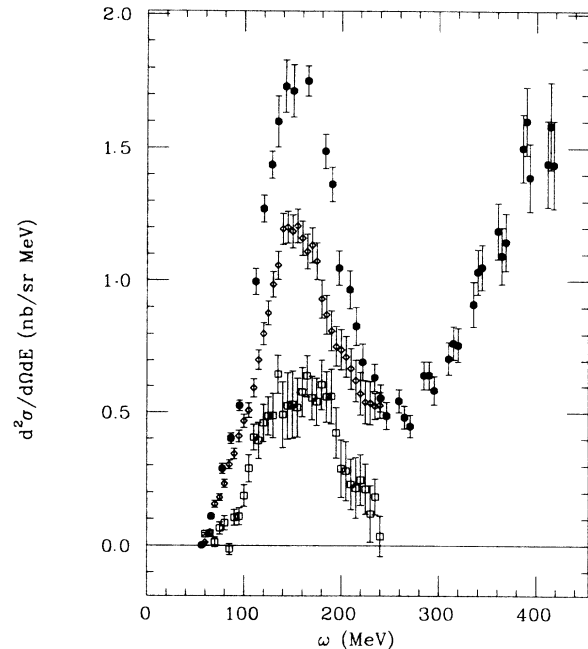

FIG. 5. Double-differential cross section for electron scattering from ^{4}He at $E = 589$ MeV, 60° (filled circles), together with the separated transverse and longitudinal components (open diamonds and squares, respectively).

procedure. The experimental results are also given in Table I. For comparison with theory, especially sum rule considerations, L/T separations provide a useful method to focus on charge and current distributions, respectively. The large discrepancy at the quasielastic peak is now seen
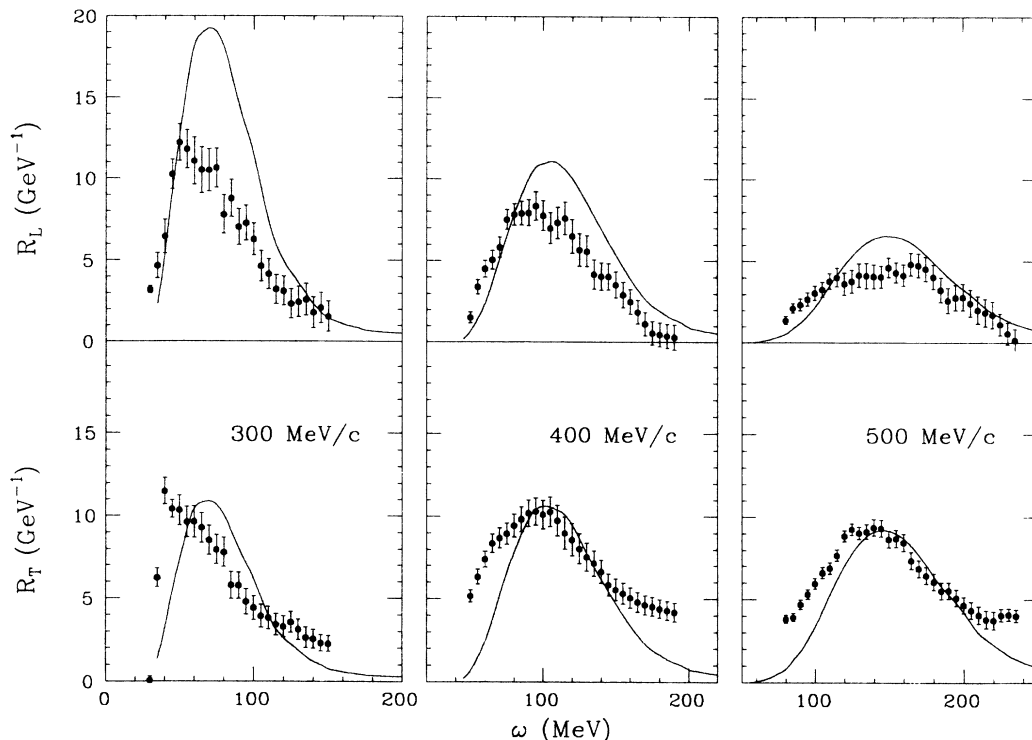

FIG. 6. Longitudinal and transverse response functions at $q = 300$, 400, 500 MeV/c together with the PWIA calculations from Ciofi degli Atti, Pace, and Salmé (Ref. 11).

TABLE I. Response functions for ^{4}He at $q = 300$, 400, and 500 MeV/c. Only relative errors are quoted. The absolute error is $\pm 8\%$. $aE - n$ denotes $a \times 10^{-n}$.

ω (MeV)	R_L (MeV^{-1})	ΔR_L (MeV^{-1})	R_T (MeV^{-1})	ΔR_T (MeV^{-1})
		$q = 300$ MeV/c		
30.0	$0.321E-02$	$0.216E-03$	$0.694E-04$	$0.238E-03$
35.0	$0.466E-02$	$0.777E-03$	$0.624E-02$	$0.562E-03$
40.0	$0.645E-02$	$0.103E-02$	$0.115E-01$	$0.809E-03$
45.0	$0.103E-01$	$0.907E-03$	$0.104E-01$	$0.543E-03$
50.0	$0.122E-01$	$0.114E-02$	$0.103E-01$	$0.915E-03$
55.0	$0.118E-01$	$0.119E-02$	$0.962E-02$	$0.921E-03$
60.0	$0.111E-01$	$0.144E-02$	$0.964E-02$	$0.948E-03$
65.0	$0.105E-01$	$0.141E-02$	$0.928E-02$	$0.891E-03$
70.0	$0.105E-01$	$0.131E-02$	$0.853E-02$	$0.881E-03$
75.0	$0.106E-01$	$0.120E-02$	$0.796E-02$	$0.890E-03$
80.0	$0.779E-02$	$0.117E-02$	$0.780E-02$	$0.888E-03$
85.0	$0.878E-02$	$0.114E-02$	$0.578E-02$	$0.825E-03$
90.0	$0.704E-02$	$0.110E-02$	$0.576E-02$	$0.804E-03$
95.0	$0.727E-02$	$0.107E-02$	$0.479E-02$	$0.770E-03$
100.0	$0.628E-02$	$0.977E-03$	$0.441E-02$	$0.712E-03$
105.0	$0.464E-02$	$0.934E-03$	$0.392E-02$	$0.683E-03$
110.0	$0.416E-02$	$0.918E-03$	$0.382E-02$	$0.676E-03$
115.0	$0.323E-02$	$0.878E-03$	$0.342E-02$	$0.648E-03$
120.0	$0.313E-02$	$0.884E-03$	$0.328E-02$	$0.635E-03$
125.0	$0.234E-02$	$0.898E-03$	$0.356E-02$	$0.618E-03$
130.0	$0.246E-02$	$0.933E-03$	$0.312E-02$	$0.616E-03$
135.0	$0.260E-02$	$0.974E-03$	$0.264E-02$	$0.617E-03$
140.0	$0.180E-02$	$0.962E-03$	$0.256E-02$	$0.567E-03$
145.0	$0.209E-02$	$0.939E-03$	$0.231E-02$	$0.494E-03$
150.0	$0.156E-02$	$0.947E-03$	$0.227E-02$	$0.471E-03$
		$q = 400$ MeV/c		
50.0	$0.153E-02$	$0.341E-03$	$0.516E-02$	$0.360E-03$
55.0	$0.341E-02$	$0.448E-03$	$0.633E-02$	$0.447E-03$
60.0	$0.451E-02$	$0.511E-03$	$0.740E-02$	$0.498E-03$
65.0	$0.506E-02$	$0.570E-03$	$0.837E-02$	$0.560E-03$
70.0	$0.584E-02$	$0.616E-03$	$0.869E-02$	$0.608E-03$
75.0	$0.753E-02$	$0.614E-03$	$0.895E-02$	$0.627E-03$
80.0	$0.783E-02$	$0.668E-03$	$0.943E-02$	$0.683E-03$
85.0	$0.791E-02$	$0.724E-03$	$0.982E-02$	$0.743E-03$
90.0	$0.794E-02$	$0.799E-03$	$0.102E-01$	$0.807E-03$
95.0	$0.835E-02$	$0.873E-03$	$0.103E-01$	$0.830E-03$
100.0	$0.776E-02$	$0.909E-03$	$0.101E-01$	$0.864E-03$
105.0	$0.699E-02$	$0.948E-03$	$0.103E-01$	$0.901E-03$
110.0	$0.732E-02$	$0.964E-03$	$0.975E-02$	$0.926E-03$
115.0	$0.759E-02$	$0.100E-02$	$0.900E-02$	$0.956E-03$
120.0	$0.650E-02$	$0.102E-02$	$0.860E-02$	$0.972E-03$
125.0	$0.567E-02$	$0.995E-03$	$0.805E-02$	$0.928E-03$
130.0	$0.559E-02$	$0.945E-03$	$0.755E-02$	$0.858E-03$
135.0	$0.418E-02$	$0.884E-03$	$0.716E-02$	$0.780E-03$
140.0	$0.405E-02$	$0.832E-03$	$0.664E-02$	$0.708E-03$
145.0	$0.404E-02$	$0.793E-03$	$0.585E-02$	$0.662E-03$
150.0	$0.354E-02$	$0.784E-03$	$0.555E-02$	$0.649E-03$
155.0	$0.293E-02$	$0.770E-03$	$0.533E-02$	$0.631E-03$
160.0	$0.251E-02$	$0.754E-03$	$0.506E-02$	$0.613E-03$
165.0	$0.188E-02$	$0.739E-03$	$0.480E-02$	$0.594E-03$
170.0	$0.113E-02$	$0.730E-03$	$0.463E-02$	$0.581E-03$
175.0	$0.568E-03$	$0.726E-03$	$0.453E-02$	$0.565E-03$
180.0	$0.477E-03$	$0.735E-03$	$0.440E-02$	$0.560E-03$
185.0	$0.383E-03$	$0.749E-03$	$0.429E-02$	$0.562E-03$
190.0	$0.305E-03$	$0.769E-03$	$0.419E-02$	$0.565E-03$

TABLE I. (Continued).

ω (MeV)	R_L (MeV^{-1})	ΔR_L (MeV^{-1})	R_T (MeV^{-1})	ΔR_T (MeV^{-1})
		$q = 500$ MeV/c		
80.0	0.139E−02	0.251E−03	0.382E−02	0.226E−03
85.0	0.215E−02	0.295E−03	0.393E−02	0.235E−03
90.0	0.237E−02	0.373E−03	0.469E−02	0.289E−03
95.0	0.271E−02	0.403E−03	0.532E−02	0.288E−03
100.0	0.309E−02	0.425E−03	0.595E−02	0.309E−03
105.0	0.329E−02	0.455E−03	0.661E−02	0.346E−03
110.0	0.380E−02	0.465E−03	0.689E−02	0.352E−03
115.0	0.404E−02	0.563E−03	0.768E−02	0.350E−03
120.0	0.365E−02	0.667E−03	0.886E−02	0.336E−03
125.0	0.379E−02	0.691E−03	0.926E−02	0.352E−03
130.0	0.417E−02	0.713E−03	0.904E−02	0.368E−03
135.0	0.414E−02	0.765E−03	0.913E−02	0.437E−03
140.0	0.409E−02	0.730E−03	0.938E−02	0.489E−03
145.0	0.407E−02	0.662E−03	0.933E−02	0.499E−03
150.0	0.463E−02	0.600E−03	0.868E−02	0.508E−03
155.0	0.433E−02	0.615E−03	0.871E−02	0.524E−03
160.0	0.417E−02	0.651E−03	0.847E−02	0.526E−03
165.0	0.484E−02	0.686E−03	0.737E−02	0.522E−03
170.0	0.476E−02	0.722E−03	0.687E−02	0.515E−03
175.0	0.455E−02	0.733E−03	0.645E−02	0.508E−03
180.0	0.406E−02	0.740E−03	0.608E−02	0.502E−03
185.0	0.328E−02	0.748E−03	0.553E−02	0.500E−03
190.0	0.263E−02	0.763E−03	0.553E−02	0.491E−03
195.0	0.280E−02	0.785E−03	0.510E−02	0.486E−03
200.0	0.283E−02	0.804E−03	0.466E−02	0.485E−03
205.0	0.245E−02	0.828E−03	0.435E−02	0.502E−03
210.0	0.204E−02	0.855E−03	0.406E−02	0.519E−03
215.0	0.188E−02	0.850E−03	0.381E−02	0.527E−03
220.0	0.173E−02	0.827E−03	0.375E−02	0.532E−03
225.0	0.114E−02	0.663E−03	0.408E−02	0.363E−03
230.0	0.577E−03	0.669E−03	0.411E−02	0.363E−03
235.0	0.170E−03	0.683E−03	0.403E−02	0.368E−03

to be largely associated with the longitudinal response at low momentum transfer. A similar qualitative feature has been seen for PWIA calculations in essentially all nuclei with no convincing explanation yet. The Saclay ^{3}He data[24] were explained by Schiavilla and Pandharipande[8] by properly orthogonalizing the final state (including some of the FSI's in the process). However, the same calculation predicted an even stronger decrease in R_L for ^{3}H, which results in worse agreement with the data than the PWIA calculation. With increasing momentum transfer, the calculations agree better with the ^{4}He data in both shape and magnitude.

For the transverse response, the peak region is better explained by the PWIA calculations except at 300 MeV/c, where the peak is significantly skewed to low-energy loss, where there are known excited states. The biggest disagreements are in the tails, where the data are much larger than the prediction. These are the regions where higher-order mechanisms are expected to contribute. Whereas final-state interactions may affect both the longitudinal and transverse responses, meson exchange currents, isobar currents, and real pion production are expected to contribute mainly to an enhancement of the

transverse response in the peak tails. However, no calculation of these effects has been made for ^{4}He. For ^{3}He, Laget included the known higher-order effects; although the response is increased on both sides of the peak, the results are not in general agreement with the Saclay data.[24]

The ^{4}He wave functions[10] that are used in the calculations[11] shown in Figs. 4 and 6 are in reasonable agreement with the charge density of ^{4}He (extracted from elastic electron scattering[25]) for $r \geq 1$ fm if MEC corrections are calculated. However, the high-momentum behavior of the form factor is not well described. In principle, the data reported here could constrain the momentum density if the contribution of higher-order effects was either small or known. At this stage, neither condition seems to hold. A somewhat independent test involves the ^{4}He($e,e'p$) reaction cross section at $q > 400$ MeV/c, where the reaction mechanism is largely quasielastic. A factorized DWIA analysis of the Nationaal Instituut voor Kunfysica en Hoge-Energiefysica (NIKHEF) data[26] indicates the Akaishi momentum densities are too small by a significant factor at momenta of 200–300 MeV/c.

The data presented here clearly point out the deficiencies of the present level of understanding the elec-

tromagnetic reaction mechanism in the ^{4}He nucleus. When the effects mentioned earlier have been accounted for, a more careful assessment can be made.

VII. COULOMB SUM RULE

The proper treatment of higher-order effects like FSI's and MEC's is the main difficulty in theoretical calculations of response functions, especially for heavier nuclei $(A \geq 4)$, where realistic wave functions for the continuum are unavailable. One way to overcome this problem and to gain more insight into the nuclear dynamics is through the consideration of sum rules. Using the closure approximation, all final-state wave functions are integrated out and these quantities then depend only on properties of the ground state. The Illinois group[9] has calculated sums for the longitudinal response. Their calculations are based on variational Monte Carlo (VMC) wave functions with two- and three-nucleon potentials. Some of the parameters of the three-nucleon force are determined by a fit to the ^{3}H and ^{4}He binding energies and to the saturation properties of nuclear matter. The main prediction by these calculations is a quenching of the Coulomb sum at momentum transfers around the typical nucleon momentum due to two-particle ground-state correlations. Neglecting contributions from the neutrons, the Coulomb sum, Σ_L, is obtained[9,12] as

$$\Sigma_L(q) = Z(1 - |F_{el}(q)|^2) + Z(Z-1)[\tilde{\rho}(q) - |F_{el}(q)|^2] .$$

$$F_{el}(q) = F_{ch}(q)/G_e^p(Q^2)$$

is the nuclear charge form factor for point nucleons, where F_{ch} is the nuclear charge form factor, G_e^p is the proton charge form factor, and

$$Q^2 = \omega_{qe}^2 - q^2 .$$

$\tilde{\rho}(q)$ is a Fourier transform of the two-proton charge density $\rho_{pp}(r,r')$. For an uncorrelated wave function, $\tilde{\rho}(q)$ will be equal to $|F_{el}(q)|^2$. In this case, the sum rule is reduced to the first term in the preceding equation:

$$\Sigma_L^{uc}(q) = Z(1 - |F_{el}(q)|^2) .$$

At momentum transfers larger than about twice the average nucleon momentum, the effect of correlations should be significantly decreased, the elastic form factor is negligible, and the Coulomb sum should then equal the target charge.

For comparison with theory the experimental Coulomb sum is formed:

$$\Sigma_L^{exp}(q) = \sum_{\omega_{min}}^{\omega_{max}} \frac{R_L^{exp}(q,\omega)\Delta\omega}{[G_E^p(Q^2)]^2 D(Q^2)} ,$$

where $Q^2 = \omega^2 - q^2$. The proton charge form factor used here is the parametrization 8.2 from Ref. 21. The change due to other possible choices of the form factor (including the dipole form) is at most 3%. The factor $D(Q^2)$ in the denominator is a correction suggested by Donnelly, Kronenberg, and van Orden[27] in order to account for relativistic effects due to the motion of the proton in the nucleus. In lowest order, $D(Q^2)$ is identical to the correction proposed earlier by deForest.[28] The two prescriptions differ by less than 1% for the situation here. This

factor leads to an increase of the sum of $\approx 5\%$.

It is obvious that the main problem in determining the experimental Coulomb sum lies in the upper summation limit ω_{max}. In most cases this limit is somewhere in the "dip" region, at roughly half the value of the photon point, $\omega = q$. If at that limit the longitudinal response is nonzero, some strength has to be assumed at higher ω values. For the very light nuclei, this is easier than for heavier nuclei because the quasielastic peak is narrower. Even the determination of the data limit itself is nontrivial since the transverse response in the "dip" is much larger than the longitudinal response (see Fig. 5). Therefore, the Rosenbluth separation results in a larger inaccuracy of the longitudinal response, especially in the dip. The values scatter around zero and may even go negative at some point. A cutoff has to be made at a physically reasonable point. We used the following methods to determine the missing strength above a given cutoff point: (i) An exponential tail was attached to the data matching the slope at the cutoff point and the extrapolated data were summed up to photon point. (The data near the cutoff point in ω have a rate of decrease that is close to exponential, with decay parameter nearly independent of q.) (ii) A second method[9] makes use of the energy-weighted sum rule (EWSR) that is obtained by multiplying the integrand in the expressions for Σ_L by ω. Like the Coulomb sum it can be calculated exactly from ground-state expectation values.[9] The experimental energy-weighted integral was determined for the range from ω_{min} to the cutoff point and compared to the theoretical value from Ref. 9. The difference is a measure of the missing strength above the cutoff if the calculated EWSR is correct. Again assuming an exponential shape of the data curve above the cutoff point, a decay parameter was fit to the calculated EWSR to give an estimate of the missing strength.

An example showing the different methods is given in Fig. 7 for the longitudinal response at 450 MeV/c. Using the error bars as limiting margins for possible extrapolations (shaded region), the solid curve is the extrapolation
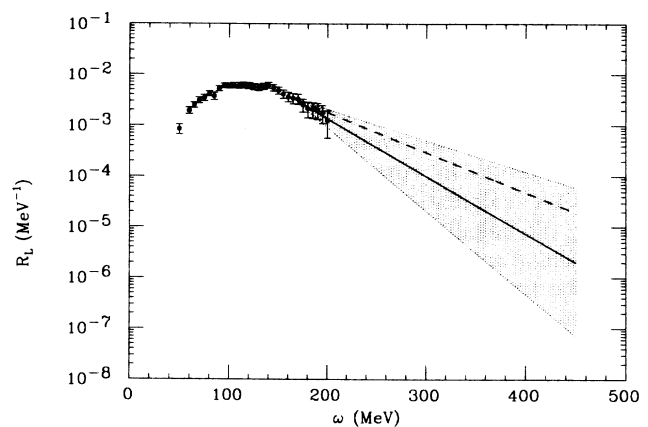

FIG. 7. Longitudinal response function at $q = 450$ MeV/c. The shaded region depicts the range of reasonable extrapolations as suggested by the error bars of the last data points. Solid curve: extrapolation as smooth continuation of the last data points. Dashed curve: extrapolation derived from the energy-weighted sum rule (EWSR).

due to the first method and the dashed curve uses the EWSR method. With $\omega = 165$ MeV as the attachment point, extrapolation with the first method results in a Coulomb sum of 1.80, the EWSR extrapolation produces 1.88, and the integration up to the data limit yields 1.77, compared to a theoretical value of 1.86 (taking into account correlations). Figure 8 shows the longitudinal response functions at constant q values between 300 and 500 MeV/c together with the exponential tails from both methods described before. The EWSR tail (dashed curve) is always higher than the exponential extrapolation (solid curve) but never outside the error bars of the last data points.

The Coulomb sum divided by Z is displayed in Fig. 9 together with the Illinois calculations. The solid curve reflects the presence of ground-state correlations, whereas the dashed curve describes the case of vanishing correlations. The error bars depict the overall experimental uncertainty that is dominated by the systematic error. The three different symbols represent (in ascending magnitude) summation (i) to the data limit, (ii) to the photon point with exponential extrapolation, (iii) to the photon point with exponential tail determined by the EWSR.
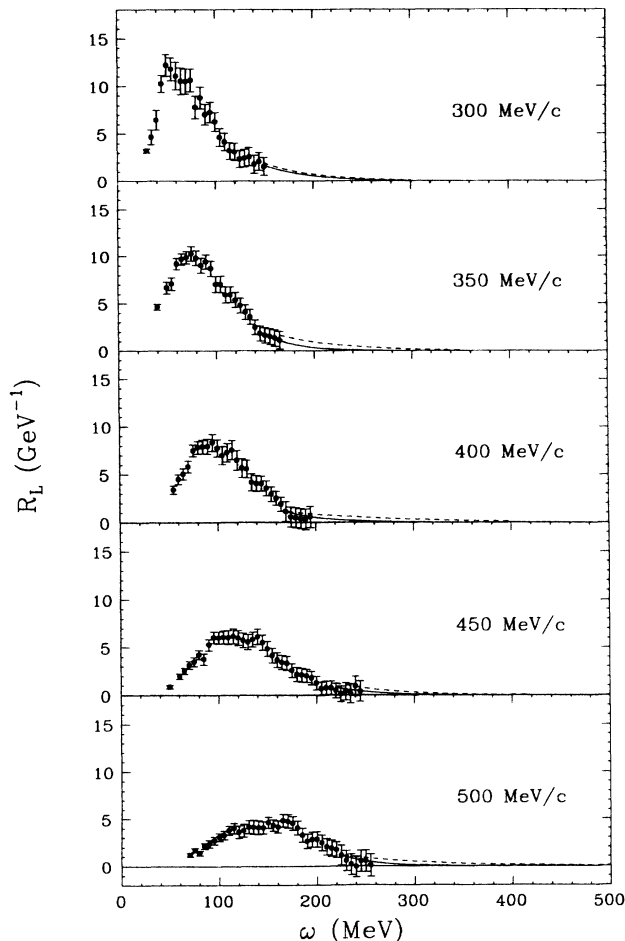
The sums to the data limit are typically lower than the Illinois results for ground-state correlations by about 10–20 %. This difference is considerably higher than that reported for the three nucleon systems[5] and is more in line with the observations for heavier nuclei in comparison with nuclear matter calculations.[9] The exponential extrapolation produces experimental values for the sum in agreement with the calculations within our stated errors, but the data points are systematically low by a few percent. The EWSR tail method gives data points slightly higher than the exponential extrapolation method, and the agreement with the Illinois calculations is similar for the two methods. We do not know with certainty whether the EWSR calculation or any other calculation involving the ^{4}He ground state is correct. Therefore, there is no way to unambiguously determine a correct method for the extrapolation. Without any other experimental information available to us, the smooth continuation of the measured data appears to be the most reasonable method to obtain a measurement of the sum rule.

Good agreement of the experimental and theoretical sum rules is observed here. If the elastic data at the same momentum transfer is equally well described by the Illinois calculations, this is a strong confirmation of the ability to evaluate the effect of ground-state pair correlations in the ^{4}He wave function. Similar conclusions have been drawn in the case of the three-body nuclei.[5] However, the exact form of these correlations cannot be derived from the data at the present level of accuracy. According to Ref. 9, a precision of 1% will be required to determine whether the proton-proton pair distribution has a central depression in the framework of their calculations. However, one has to keep in mind that some of the theoretical assumptions used in the calculations are only accurate at the 5% level.

VIII. CONCLUSIONS

The inelastic electron scattering data presented in this paper are the first to cover a substantial portion of the in-

FIG. 8. Longitudinal response functions at momentum transfers between 300 and 500 MeV/c. Extrapolations up to the photon point are also shown: EWSR (dashed curve), smooth continuation of data (solid curve).
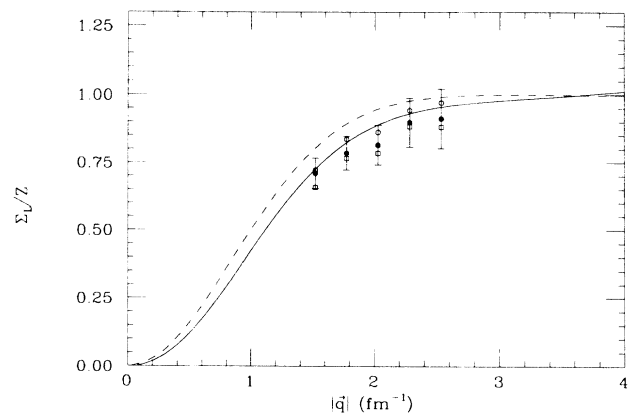

FIG. 9. Coulomb sum rule for ^{4}He. The open diamonds represent summation up to the data limit. The summation of the smoothly extrapolated data is given by filled circles. The results for EWSR-extrapolated data are shown as open circles. The error bars include random and systematic uncertainties. The solid curve is the ground-state correlations calculation by Ref. 9 and the dashed curve is the no-correlations limit.

termediate energy (q,ω) plane for ^{4}He. Model-independent radiative corrections were obtained in a self-consistent method. For the first time for this nucleus, the substantial body of data presented here allowed the determination of model-independent longitudinal-transverse response separations at momentum transfers from 300 to 500 MeV/c. Calculations[11] based on the PWIA clearly fail to describe the reaction mechanism at the low momentum transfers and are in fair agreement with the data at the higher q values. The most severe discrepancies are seen in the longitudinal response near the peak of the distribution. This is quite similar to the problems seen with nuclei of lighter mass[5] (^{3}H and ^{3}He) and higher mass.[2] It is quite surprising since the known many-body effects will predominantly influence the transverse response. No convincing explanation has yet been found for these phenomena, but data for the lightest nuclei will clearly play an important role in any future understanding.

There have been questions whether nuclear models with only nucleon degrees of freedom are sufficient to explain nuclei. An important clue comes from the Coulomb sum data. This quantity is insensitive to effects in the final state that have proven difficult to calculate. Only the distribution and correlations of charges in the ground-state wave function are being tested. The data clearly disagrees with the calculation with no correlations. Calculations[9] using wave functions derived from conventional two- and three-nucleon forces are in good agreement with the ^{4}He data. Similar calculations for ^{3}He and ^{3}H agreed well, also.[5] Thus, wave functions assuming only nucleon degrees of freedom are able to describe the overall effect of charge correlations in these light nuclei.

ACKNOWLEDGMENTS

*Present address: McLean Laboratory, Woods' Hole Oceanographic Institute, Woods' Hole, MA 02543.

†Present address: Physics Department, University of Illinois, Champaign, IL 61820.

‡Present address: Department of Physics, University of Lund, S-223 62 Lund, Sweden.

§Present address: NIKHEF-K, Amsterdam, The Netherlands.

**Present address: Physics Department and Bates Linear Accelerator Center, Massachusetts Institute of Technology, Cambridge, MA 02139.

††Present address: Continuous Electron Beam Accelerator Facility, Newport News, VA 23606.

[1] E. J. Moniz, Phys. Rev. 184, 1154 (1969); E. J. Moniz *et al.*, Phys. Rev. Lett. 26, 445 (1971); R. R. Whitney *et al.*, Phys. Rev. C 9, 2230 (1974).

[2] P. Barreau *et al.*, Nucl. Phys. A402, 515 (1983); Z. E. Meziani *et al.*, Phys. Rev. Lett. 52, 2130 (1984); M. Deady *et al.*, Phys. Rev. C 33, 1897 (1986); C. C. Blatchley *et al.*, *ibid.* 34, 1243 (1986).

[3] B. P. Quinn *et al.*, Phys. Rev. C 37, 1609 (1988); S. A. Dytman *et al.*, *ibid.* 38, 800 (1988); B. P. Quinn, Ph.D. thesis, Massachusetts Institute of Technology, 1984.

[4] W. Fabian and H. Arenhövel, Nucl. Phys. A314, 253 (1979); H. Arenhövel, *ibid.* A384, 287 (1982); J. M. Laget, Can. J. Phys. 62, 1046 (1984).

[5] K. Dow *et al.*, Phys. Rev. Lett. 61, 1706 (1988); K. Dow, Ph.D. thesis, Massachusetts Institute of Technology, 1987; T. Ueng, Ph.D. thesis, University of Virginia, 1988; A. M. Bernstein, in *Perspectives in Nuclear Physics at Intermediate Energies, Trieste, Italy, 1987*, edited by S. Boffi, C. Ciofi degli Atti, and M. M. Giannini (World Scientific, Hong Kong, 1988); S. A. Dytman, in *Quarks, Mesons, and Nuclei*, Vol. II of *Proceedings of the Spring School on Medium- and High-Energy Nuclear Physics, Taipei, Taiwan, 1988*, edited by W.-Y. Pauchy Hwang and E. M. Henley (World Scientific, Hong Kong, 1989), p. 65.

[6] H. Meier-Hajduk *et al.*, Nucl. Phys. A395, 332 (1983).

[7] C. Ciofi degli Atti, E. Pace, and G. Salmé, Phys. Lett. 127B, 303 (1983); and private communication.

[8] R. Schiavilla and V. R. Pandharipande, Phys. Rev. C 36, 2221 (1987).

[9] R. Schiavilla *et al.*, Nucl. Phys. A473, 267 (1987).

[10] Y. Akaishi, Nucl. Phys. A416, 409c (1984).

[11] C. Ciofi degli Atti, Nucl. Phys. A463, 127c (1987); G. Salmé and E. Pace, private communication.

[12] T. deForest and J. D. Walecka, Adv. Phys. 15, 1 (1966).

[13] W. Bertozzi *et al.*, Nucl. Instrum. Methods 162, 211 (1979), and references therein.

[14] K. von Reden, Bull. Am. Phys. Soc. 32, 1059 (1987); A. M. Bernstein *et al.* (submitted to Phys. Lett.).

[15] D. Beck *et al.*, Nucl. Instrum. Methods A277, 323 (1989); G. A. Retzlaff, Nucl. Instrum. Methods B24/25, 950 (1987).

[16] Registered trademark of the Elgiloy Company, Elgin, Illinois.

[17] W. E. Keller, *Helium-3 and Helium-4* (Plenum, New York, 1969), p. 40; M. Farkondeh, Massachusetts Institute of Technology report, 1987.

[18] L. W. Mo and Y. S. Tsai, Rev. Mod. Phys. 41, 205 (1969); G. Miller, Stanford Linear Accelerator Center Report No. 129, 1971.

[19] R. F. Frosch *et al.*, Phys. Rev. 160, 874 (1967).

[20] T. deForest, Jr., Nucl. Phys. A392, 232 (1982).

[21] G. Höhler *et al.*, Nucl. Phys. B114, 505 (1976).

[22] S. Blatnik and N. Zovko, Acta Phys. Austriaca 39, 62 (1974).

[23] M. Gari and W. Krümpelmann, Z. Phys. A 322, 689 (1985).

[24] C. Marchand *et al.*, Phys. Lett. 153B, 29 (1985).

[25] I. Sick, in *Few Body Systems and Electromagnetic Interactions*, Vol. 86 of *Lecture Notes in Physics*, edited by C. Ciofi degli Atti and E. DeSanctis (Springer-Verlag, Berlin, 1978), p. 299; J. McCarthy *et al.*, Phys. Rev. C 15, 1396 (1977).

[26] J. F. J. van den Brand, Ph.D. thesis, Vrije Universiteit, 1988; J. F. J. van den Brand *et al.*, Phys. Rev. Lett. 60, 2006 (1988).

[27] T. W. Donnelly, E. I. Kronenberg, and J. W. van Orden, Nucl. Phys. A494, 365 (1989).

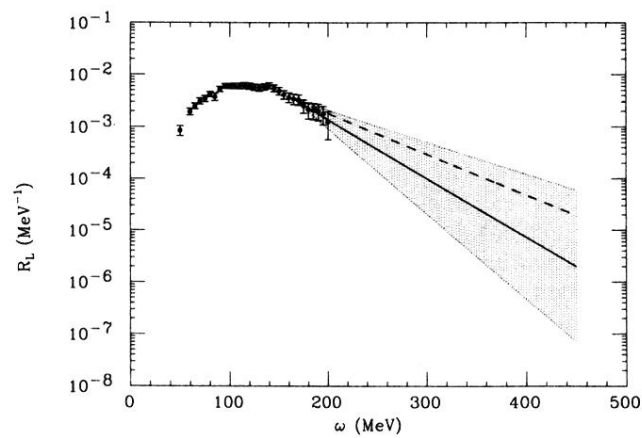[28] T. deForest, Nucl. Phys. A414, 347 (1984).

FIG. 7. Longitudinal response function at $q = 450$ MeV/c. The shaded region depicts the range of reasonable extrapolations as suggested by the error bars of the last data points. Solid curve: extrapolation as smooth continuation of the last data points. Dashed curve: extrapolation derived from the energy-weighted sum rule (EWSR).